Van der Pauw measurement of metal fibre orientation in a plastic–metal composite

MARK KINSLER
Electrical Engineering Department, University of Pittsburgh, Pittsburgh, Pennsylvania 15260, USA

LAWRENCE V. HMURCIK*, JOYCE PATTON
Electrical Engineering Department, University of Bridgeport, Bridgeport, Connecticut 06601, USA

Stainless steel fibres in ABS plastic form a composite with an anisotropic resistivity. Samples are rectangular shapes with uniform thickness. By assuming two principal resistivities and by using van der Pauw's technique, we find $\varrho^2 = \varrho_x \varrho_y$. For rectangular samples, field theory determines ϱ_y / ϱ_x and hence fibre direction. Results for three sample geometries agree with the theoretical predictions of the fibre patterns and with X-ray data. Samples formed by a centre-sprue feed are the best for fabricating large, uniform samples, while samples with a large length-to-width ratio have the most uniform metal density and fibre orientation. Resistivity was also measured by the more-common two-probe technique. Results correlate well to van der Pauw data, with 95% confidence.

1. Introduction

Much work has been done to study composites consisting of a plastic matrix with metal or carbon filler. Such composites can be used to construct housings to shield circuits from electromagnetic interference (EMI); they are easy to fabricate and machine, and they are lighter than metal [1, 2].

Characterization of a composite is usually done by measuring its resistivity (ϱ). Other material parameters, such as the dielectric constant, can also be used to characterize a composite, but they are usually not as easy to measure as the resistivity. It has been shown by many authors that as the percentage of metal (or carbon) is increased, the composite passes through a percolation limit, wherein ϱ may drop six or more orders of magnitude [1]. Low resistivity corresponds to a large shielding effectiveness, where we define the shielding effectiveness at a given frequency as the decibel ratio of transmitted to incident EMI.

We measured ϱ by the van der Pauw technique [3–5]. Resistivity is found by solving

$$\exp\left(RV_{AB}/I_{CD}\right) + \exp\left(RV_{BC}/I_{DA}\right) = 1 \quad (1)$$

where $R = -\pi d / \varrho$, d is the sample thickness (0.327 cm for all of our samples), and I and V are current and voltage, respectively. In practice, we cut our samples to a rectangular shape and place a contact at each corner. If we label each contact A, B, C, D proceeding clockwise, then $V_{AB}(V_{BC})$ is the voltage measured across points AB(BC) when a current passes through points CD(DA). Contact A is located in the upper left-hand corner.

The van der Pauw method assumes that the samples being studied are homogeneous and isotropic. For non-homogeneous samples, ϱ is the average resistivity [5]. For samples which are anisotropic, we can define the principal resistivities along the x- and y-axes. Resistivity is the geometric mean [6]

$$\varrho^2 = \varrho_x \varrho_y \quad (2)$$

We studied the anisotropy of metal fibres in a plastic matrix as a function of its moulding geometry. Our samples were Magnex™, obtained from Mitech Corporation, Willoughby, Ohio. They are ABS plastic with stainless steel fibres (nos 304 and 316), loaded to 1% by volume. Fibres are 7 μm diameter and have a typical aspect ratio of 200 [7]. Commercially available samples of Magnex have a resistivity of less than 1 Ω cm. Samples provided for this study include some with higher resistivity values.

We used current and voltage measurements to calculate the average resistivity in Equation 1. As our samples are rectangular, let $K = \varrho_y / \varrho_x$, and find K using image currents and potential-field mapping techniques [8]. This requires no new measurements. Data taken by van der Pauw's method are sufficient. K can be found by solving either of two equations:

$$\exp\left(-DV_{AB}/I_{CD}\right) = \prod_{n=0}^{\infty} \tanh\left[Q(n + 0.5)\pi\right] \quad (3)$$

and

$$\exp\left(-DV_{BC}/I_{DA}\right) = \prod_{n=0}^{\infty} \tanh\left[(n + 0.5)\pi/Q\right] \quad (4)$$

---

*Author to whom all correspondence should be addressed.

where $Q = Kb/a$, $D = \pi d/8\varrho$, a is the sample width along the x-axis, and b is the sample length along the y-axis.

Equations 3 and 4 are consistent with each other. Solution of either equation for the same sample should give us the same K value. In practice, measurement errors will cause each value of K to differ slightly. By solving to find both a value for K and an error, K can be determined in an unambiguous way, generally as an average of the two values. Errors in the measurement of K are typically less than 1%, while errors in resistivity are about 2% or less.

Errors in geometry (a, b, d) and electronic measurement (I, V) tend to be small ($\sim 0.1\%$) compared to the error in the calculation of ϱ ($\sim 2\%$). Therefore,

$$\sigma_K = \frac{KdV_{AB}\sigma_\varrho}{4I_{CD}\varrho^2 Q} \left[\sum_{n=0}^{\infty} \frac{2n + 1}{\sinh[(2n + 1)\pi Q]} \right]^{-1} \quad (5)$$

and

$$\sigma_K = \frac{KdV_{BC}\sigma_\varrho Q}{4I_{DA}\varrho^2} \left[\sum_{n=0}^{\infty} \frac{2n + 1}{\sinh[(2n + 1)\pi/Q]} \right]^{-1} \quad (6)$$

The error in the measurement of resistivity is caused by the non-zero width (1 mm) of our contacts and by the fact that they are recessed 1 mm from the sample perimeter. This error has been analysed [3, 9, 10], and we use these results to obtain a maximum theoretical error of $(\sigma\varrho/\varrho) = 0.5\%$. We also measured the experimental error. We applied 20 contacts each to the perimeter of five Magnex plaques (15 cm $\times$ 7.5 cm $\times$ 0.327 cm). Using four contacts at a time to measure ϱ, we obtain the percentage error as the standard deviation divided by the average. Maximum error was 2%. We used the larger percentage error in our analysis.

In Equations 5 and 6, if the sample is a square with isotropic fibre distribution, then $Q = K = 1$, and Equations 5 and 6 are the same. (Equations 3 and 4 would also be the same.) For all other cases, the errors in K would be different. In Table I, we list results for some of the data used in this paper. K values differ by about 1% or less. An average value and range of error are determined in each case. Specific sample pieces and their geometry are discussed in the following sections.

TABLE I Values of K, plus or minus one σ, are determined using Equations 3, 7 and 4, 8. Sample resistivity is also listed. Data are selected at random for each piece listed

Sample		K (3, 7)	K (4, 8)	ϱ (Ω cm)
Plaque	1	0.754 $\pm$ 0.009	0.754 $\pm$ 0.010	0.575
	5	2.39 $\pm$ 0.02	2.33 $\pm$ 0.05	0.493
	7	0.142 $\pm$ 0.003	0.142 $\pm$ 0.001	1.15
	8	0.767 $\pm$ 0.009	0.760 $\pm$ 0.010	0.925
Paddle	3	1.82 $\pm$ 0.01	1.81 $\pm$ 0.04	3.25
	4	0.349 $\pm$ 0.006	0.345 $\pm$ 0.003	0.719
	15	1.53 $\pm$ 0.01	1.51 $\pm$ 0.03	0.719
	16	0.582 $\pm$ 0.001	0.584 $\pm$ 0.007	5.33
Dogbone	1	0.530 $\pm$ 0.003	0.529 $\pm$ 0.012	2.63
	4	0.191 $\pm$ 0.001	0.191 $\pm$ 0.005	0.791
Carbon	1	0.217 $\pm$ 0.002	0.214 $\pm$ 0.003	0.544
	5	0.962 $\pm$ 0.012	0.958 $\pm$ 0.012	2.13
	8	1.38 $\pm$ 0.01	1.38 $\pm$ 0.02	2.09

2. Orientation studies

We obtained Magnex samples moulded in three different geometries. The fibre orientation for each geometry was studied by cutting each sample into small rectangular pieces and finding ϱ and K for each piece. Contacts (1 mm diameter) were driven into each piece at their corners [11].

We model each sample piece by a number of straight lines. The density of lines tells the metal fibre density, which varies inversely with the sample's resistivity. Lines are oriented at an angle θ relative to the x-axis, where

$$\theta = \tan^{-1}(1/K) \quad (7)$$

and this tells the principal orientation of the fibres. Modelling our fibre patterns in this manner is equivalent to defining a current density of fibre.

There are three problems with our modelling process.

1. If a sample is anisotropic, most fibres will have an orientation angle θ, but there will still be a number of fibres orientated at other angles. By using Equation 5, we find an equivalent orientation for all fibres. In our Magnex samples, the volume percentage of metal (0.01) is greater than the inverse of the aspect ratio. This criterion forces the fibres in each sample to pack together into tight parallel bunches [12]. The large fibre aspect ratio (~ 200) makes the plastic a highly concentrated solution which in turn forces the fibre pattern to be highly anisotropic [13]. Thus, each parallel bundle will have a single orientation angle θ, while each fibre in the bundle deviates from θ.

2. We model our fibre pattern using straight lines. However, most fibre patterns tend to curve throughout a sample. By dividing a sample into small pieces and by measuring the fibre orientation of each piece, we can approximate the curvature by a series of straight lines. These straight lines can then be "smoothed out" by curve fitting techniques used in the study of two-dimensional electric field mapping [14].

3. The third problem with our modelling process is the most serious. Given a value of ϱ and K, we can find θ, but we cannot determine an unambiguous reference axis. For example, let $\theta = 20°$, and let the resistivity be represented by five complete lines per unit area. With this information, we can produce any of the four patterns shown in Fig. 1 (plus other variations). Our ϱ and K values provide quantitative information about the fibre orientation and density relative to the x and y directions. Qualitative information to distinguish the actual fibre pattern can be obtained by visual inspection [15] or by X-ray analysis [16]. Magnex samples identical to ours have been studied by X-ray analysis to determine the shape of their fibre pattern [7], and this information is employed in the present study.

2.1. Centre-sprue plaques

We obtained five Magnex plaques (7.5 cm $\times$ 15 cm) with an 8 mm wide sprue at 90° to the face of the plaque and located at its centre. During moulding, the plastic melt started at the plaque's centre and flowed outward to the edges. Shear force at the point of
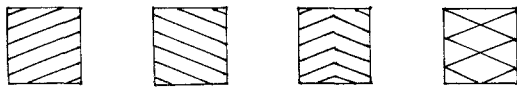
Figure 1 Four squares of unit area have the same resistivity (shown as five complete lines per square) and orientation (20°). Patterns cannot be distinguished from each other by the van der Pauw technique alone.

injection was minimized by the large diameter of the sprue. Values of ϱ and K were measured for each plaque. The plaques were then cut into 15 pieces as shown in Fig. 2a, and K and ϱ were found for each piece. An average K and ϱ (plus or minus one standard deviation) were determined for each piece by averaging each set of five values. These data are listed in Table II, and a fibre pattern based on them is shown in Fig. 2b. Fibre density at the centre of the plaque is large, i.e. resistivity is $0.763\,\Omega\,\mathrm{cm}$ for piece 8. It decreases at a distance of a few centimetres from the centre as ϱ increases. The pattern is circular and encompasses pieces 5, 7, 9 and 11. The sprue is a diverging source of plastic melt. Flow from a diverging source tries to stretch the metal fibres and this causes them to rotate into a position perpendicular to the melt flow [17]. The fibres line up as concentric circles surrounding the sprue. The amount of metal in the expanding melt wavefront remains constant. Therefore, as the front expands in larger circles, the density of metal drops and the resistivity goes up.

When the melt reaches the sample edges parallel to the y-axis, the size of the wavefront becomes constant, and its speed suddenly increases. More fibre is drawn off to fill pieces 1, 2, 3 and 13, 14, 15. A greater fibre density at the edges has been observed in other studies of Magnex [18] as well as in carbon fibre composites [1]. Fibre orientation in the two edges parallel to the x-axis resembles portions of concentric ellipsoids. The pattern shown in Fig. 2 is a straight line approximation of the pattern observed by X-ray analysis in identical samples [7]. Centre-sprue plaques are fairly uniform in their ability to shield EMI. There is a marked difference between the five samples, even though they were fabricated under identical conditions. This is noted by the large standard deviations of ϱ and K for each of the 15 pieces. Nevertheless, as the resistivity for each piece is close to unity, the whole
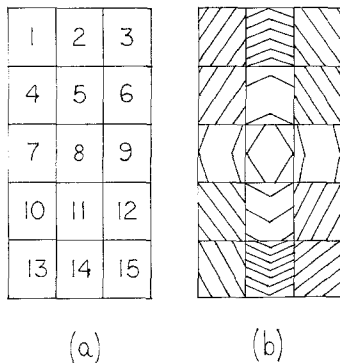
TABLE II Average and standard deviation of ϱ and K for five Magnex samples with sprue at centre. Values are for pieces identified in Fig. 2

Piece	ϱ ($\Omega\,\mathrm{cm}$)	K
Whole	0.776 ± 0.315	–
1	0.486 ± 0.158	0.677 ± 0.111
2	0.368 ± 0.074	3.16 ± 0.30
3	0.530 ± 0.085	0.674 ± 0.093
4	0.588 ± 0.095	0.658 ± 0.267
5	1.30 ± 1.05	2.41 ± 1.07
6	0.487 ± 0.127	0.605 ± 0.084
7	1.29 ± 0.59	0.303 ± 0.118
8	0.763 ± 0.337	0.681 ± 0.144
9	1.44 ± 0.53	0.191 ± 0.060
10	0.518 ± 0.039	0.746 ± 0.203
11	0.919 ± 0.425	1.69 ± 0.39
12	0.504 ± 0.105	0.503 ± 0.153
13	0.587 ± 0.166	0.503 ± 0.269
14	0.320 ± 0.074	3.29 ± 0.78
15	0.451 ± 0.120	1.28 ± 0.49

sample can provide a good shielding effectiveness over its entire surface. Typical values of shielding effectiveness are 30 to 40 dB.

2.2. Paddle

Six Magnex samples were moulded in the shape of the "paddle" shown in Fig. 3. The sprue is on the right side of the connecting tab, and it is 3 mm wide. The paddles were cut into 16 pieces. K and ϱ were measured for each piece, and a fibre pattern was developed (see Fig. 3). Table III gives the average and standard deviation of K and ϱ for each piece.

The source of plastic melt at the tab is a diverging source. This has a dramatic effect on the fibre pattern of pieces 1, 2, 3, and 4. In pieces 2 and 3, the melt front expands, tries to stretch the stainless steel fibres, and causes them to rotate to a position perpendicular to the direction of melt flow. In piece 4, not only does an expansional force play a role in fibre orientation, but also a shear force is introduced. Near the edge of the sample, fibres are forced into the vicinity of the walls of the mould. They either shear apart as they drive into the wall, or more likely, they relieve the shear by aligning parallel to the mould wall [19]. Piece 1 is unusual in that it contains virtually no fibres. Resistivity is in excess of 5000 ($\Omega\,\mathrm{cm}$). During moulding,
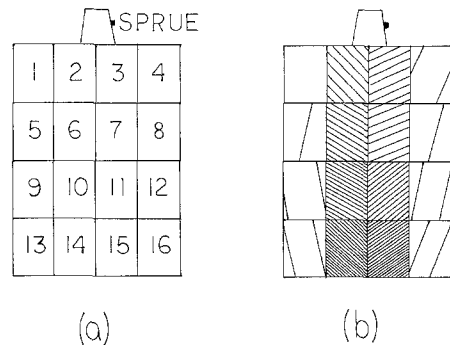

Figure 2 (a) Magnex plaque (7.5 cm × 15 cm), with the sprue at the centre, is cut into 15 identical pieces. Sprue (not shown) is 0.8 cm wide. (b) The fibre pattern is determined by van der Pauw data coupled with X-ray analysis.

Figure 3 (a) A Magnex paddle (7.5 cm × 10 cm) is cut into 16 identical pieces. Sprue is 0.3 cm wide. (b) Fibre pattern shows a greatly reduced fibre density in pieces at the edges. Piece 1 (with no metal fibre) is filled by plastic backflow during the moulding process.

TABLE III Average and standard deviation of ϱ and K for six Magnex paddles. Values are for pieces identified in Fig. 3

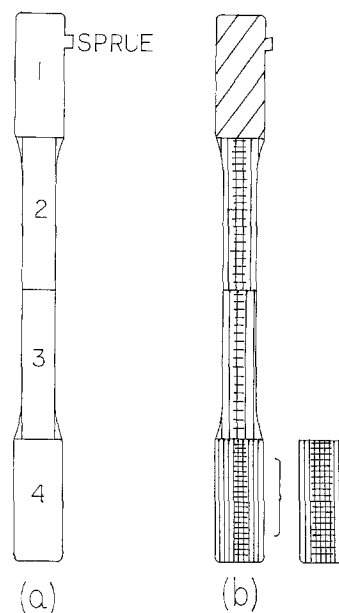| Piece	ϱ (Ω cm)	K
Whole	1.13 $\pm$ 0.35	–
1	> 5000	–
2	2.97 $\pm$ 3.16	1.01 $\pm$ 0.79
3	3.08 $\pm$ 1.58	2.27 $\pm$ 0.90
4	13.5 $\pm$ 16.6	0.369 $\pm$ 0.310
5	19.0 $\pm$ 8.9	0.157 $\pm$ 0.107
6	2.16 $\pm$ 1.39	1.68 $\pm$ 0.10
7	2.82 $\pm$ 1.72	2.46 $\pm$ 1.23
8	26.4 $\pm$ 29.4	0.219 $\pm$ 0.094
9	16.5 $\pm$ 15.4	0.131 $\pm$ 0.117
10	1.55 $\pm$ 0.59	2.14 $\pm$ 0.57
11	1.39 $\pm$ 0.88	1.57 $\pm$ 0.52
12	11.3 $\pm$ 8.0	0.169 $\pm$ 0.063
13	11.5 $\pm$ 9.9	0.219 $\pm$ 0.074
14	0.670 $\pm$ 0.369	1.12 $\pm$ 1.02
15	0.810 $\pm$ 0.077	1.51 $\pm$ 0.46
16	8.61 $\pm$ 5.38	0.372 $\pm$ 0.104

Figure 4 (a) A Magnex "dogbone" (2 cm × 22 cm) is cut into four rectangular pieces. Sprue is 0.5 cm wide. (b) Fibre pattern shows a superposition of horizontal and vertical components for pieces 2, 3 and 4. A bimodal distribution in samples for piece 4 produces the two different patterns shown.

plastic is injected at the right side of the tab. It strikes the left side, rebounds, and enters the paddle heading in a direction toward the right. It does not fill piece 1 significantly. Piece 1 is filled later in the moulding process by a backflow of plastic from pieces 5 and 6. This backflow carries virtually no metal fibres with it, and piece 1 remains an insulator.

Pieces 5 to 16 do not see the plastic flow from a diverging source. Rather, the melt appears as a constant wavefront. Experimental [19] and theoretical [20] studies have shown that the fibres are oriented parallel to the direction of flow by shear forces near the mould walls and perpendicular to the flow by expansional forces away from the walls. If the plaque width were significantly reduced, the shear force would dominate and the fibres would line up parallel to the direction of flow throughout. We will see this effect in the next section.

Resistivity values are about an order of magnitude higher for pieces on the edge than for pieces in the centre. Therefore, metal density is an order of magnitude lower at the edge. These results, coupled with those for piece 1, would indicate that the metal fibre has a large inertial drag. As the plastic from the tab travels down the y-axis and expands to the right and left, pieces on the edges are filled in with plastic which has a lower metal density than centre pieces.

The paddles are poor EMI shields. Overall, the resistivity is much larger than it was for the plaques. As both are fabricated to have the same total metal density, the increased resistivity is caused by a smaller fibre aspect ratio. The sprue is small, and injected plastic must turn sharply to fill the mould. Both factors cause fibres to break. In addition, the low fibre density at the edges relative to the centre produces large gaps in the paddle's ability to shield EMI.

2.3. Dogbone

We measured ϱ and K for eight Magnex samples in the shape of a "dogbone". The sprue is 5 mm wide, and each sample is cut into four rectangular pieces. See Fig. 4a. Average values of ϱ and K for each piece (plus or minus one standard deviation) are listed in

Table IV, with a fibre pattern drawn in Fig. 4b. During the moulding process, plastic entering the sprue must turn sharply to fill the mould. This would tend to increase fibre breakage. However, as the sprue is larger than that used to mould the paddles, breakage is reduced. This is indicated by the relatively low value of resistivity in each piece. Piece 1 has the highest ϱ value and hence the lowest fibre density.

Piece 1 has K values close to unity ($\theta \simeq 45°$). The pattern drawn in Fig. 4b indicates a uniform flow of fibre as the plastic enters the sprue, turns 90°, and leaves piece 1. In truth, the pattern is highly irregular. The pattern exhibits a high degree of vorticity. Near the top left corner, there is almost no metal. (This is similar to piece 1 for the plaque.) When making measurements, our contact in this corner had to be relocated about 2 mm inwards in order to obtain usable measurements. Thus, our values for ϱ and K contain more measurement error for piece 1 than for the other pieces.

For pieces 2, 3, 4 the fibres line up parallel to the y-axis, while a small number at the centre align parallel to the x-axis. Pieces 2 and 3, measured as one piece, have K values near zero. Thus, $\theta \approx 90°$. When the pieces are measured individually, K increases. For

TABLE IV Average and standard deviation of ϱ and K for eight Magnex samples in the shape of a "dogbone". Values are for pieces identified in Fig. 4

Piece	ϱ (Ω cm)	K
Whole	2.65 $\pm$ 0.44	–
1	1.80 $\pm$ 0.60	0.691 $\pm$ 0.150
2	0.801 $\pm$ 0.101	0.208 $\pm$ 0.011
3	0.864 $\pm$ 0.128	0.206 $\pm$ 0.032
4	0.512 $\pm$ 0.170	0.447 $\pm$ 0.037 and 0.257 $\pm$ 0.042
2 plus 3	–	0.0856 $\pm$ 0.0394

shorter pieces, the cross fibres play a greater role in determining overall fibre orientation, i.e. K. Pieces 2, 3 and 4 show a pattern which would be observed in the paddles, if the width were reduced. The effect of shear on the fibres (caused by the mould walls) extends deep into the centre of the sample and dominates over expansional forces [19].

Also, for piece 4 there is a bimodal distribution in K values. Because values of ϱ can be fitted to a single normal distribution, the amount of metal in piece 4 is relatively constant for all eight samples. Fibre orientation, however, can be fit by two distributions (in K) which do not overlap within one standard deviation. Patterns for both orientations are shown in Fig. 4b. The differing patterns are caused by the speed of the plastic melt during moulding. Plastic leaving piece 3 will diverge as it enters piece 4. This increases the effect of the expansional forces, which tends to align more fibre perpendicular to the melt flow [17]. K increases. But if the speed of melt travel is slow enough, some plastic along the edges can creep ahead of the main flow of plastic [21]. This would wet the edges near the boundary of pieces 3 and 4. The flow of plastic leaving piece 3 would not diverge. The number of cross fibres would remain essentially constant and so would K.

The standard deviations of ϱ and K are small relative to the plaque and paddle (especially for pieces 2, 3, 4). The dogbone geometry (or any long, thin geometry) provides samples which can be fabricated uniformly and which provide a large shielding effectiveness. There is only one disadvantage with this geometry. A large component made of Magnex would have to be built up of many smaller pieces laminated together.

2.4. Carbon plaques

We studied four polypropylene plaques (7.5 cm × 15 cm) loaded to 32% (volume) with carbon black powder (XC-72 by Cabot Corp., Billerica, Massachusetts). The carbon particles are roughly spherical (~ 20 nm), but during moulding they can fuse into chains with an aspect ratio as large as 5 [22]. Because the aspect ratio is small compared to Magnex, the carbon does not form a mesh network in the plastic as the stainless steel did. Rather, conduction occurs by electrons tunnelling through a thin plastic layer between adjacent carbon particles [22].

We cut our samples into 18 squares numbered as shown in Fig. 2, with three across and six down. Table V lists average values of ϱ and K for each piece and their standard deviations. The samples are homogeneous. The resistivity deviates only slightly from piece to piece and sample to sample. Also, the resistivity of each piece deviates only slightly from the resistivity of the whole sample before it is cut up. Values of about $2 \, \Omega$ cm are bracketed by the resistivity of XC-72 in ethylene vinyl acetate ($7 \, \Omega$ cm for 32% loading) [2] and in polyvinyl chloride ($1 \, \Omega$ cm for 32% loading) [23].

The orientation of carbon chains in most pieces is isotropic. Values for K are close to unity. The exceptions would be pieces 5 and 14. Carbon chains can form in all 18 pieces. However, all pieces, except 5, 8,

TABLE V Average and standard deviation of ϱ and K for four plaques of carbon-black in polypropylene. Pieces are numbered in the fashion shown in Fig. 2, with three pieces across and six pieces down

Piece	ϱ (Ω cm)	K
Whole	2.07 ± 0.08	–
1	2.18 ± 0.04	0.982 ± 0.040
2	2.22 ± 0.08	1.13 ± 0.13
3	2.26 ± 0.05	1.08 ± 0.05
4	2.14 ± 0.03	1.09 ± 0.05
5	2.08 ± 0.02	1.34 ± 0.14
6	2.12 ± 0.04	1.13 ± 0.06
7	2.10 ± 0.05	1.13 ± 0.03
8	1.97 ± 0.01	1.13 ± 0.09
9	2.13 ± 0.02	1.09 ± 0.04
10	2.12 ± 0.02	1.02 ± 0.06
11	2.00 ± 0.03	1.18 ± 0.07
12	2.10 ± 0.04	1.04 ± 0.05
13	2.07 ± 0.05	1.06 ± 0.04
14	2.07 ± 0.02	1.32 ± 0.02
15	2.13 ± 0.03	1.10 ± 0.12
16	2.19 ± 0.03	1.07 ± 0.05
17	2.22 ± 0.08	1.19 ± 0.09
18	2.20 ± 0.02	1.05 ± 0.07

11 and 14, lie at the edges. Shearing at the mould walls during formation would break apart the fragile carbon chains. Furthermore, pieces 8 and 11 enclose the centre sprue. Shear force and turbulence caused by the injection of plastic would break apart carbon chains in these pieces. Pieces 5 and 14 remain as isolated regions of calm. The expansion of plastic melt from the plaque centre causes carbon chains to align parallel to the x-axis, just as it did in the Magnex plaques. K is greater than unity. As a first approximation, K equals the aspect ratio of the carbon chains, i.e. about 1.3.

3. Conclusion

Our measurements of resistivity and resistive anisotropy via van der Pauw's method have proved valuable in determining the orientation pattern of stainless steel fibres and carbon chains. Our results correspond to pictures produced by X-ray measurements. In addition, they provide quantitative data about the fibre in any region.
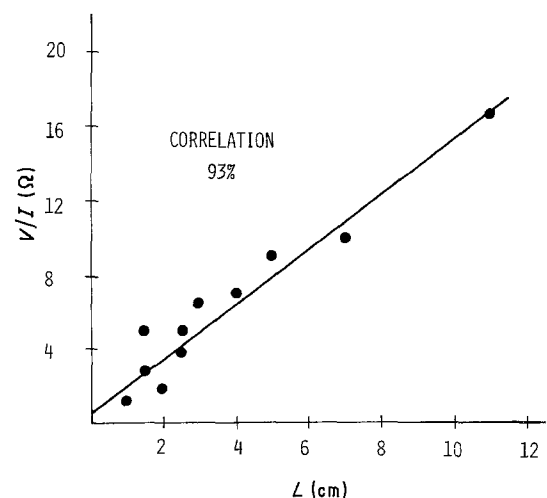

Figure 5 For the two-probe technique, the ratio of voltage to current against contact separation produces a linear relationship (93% correlation). Resistivity in the direction of current flow (ϱ_y) is extracted using linear regression.
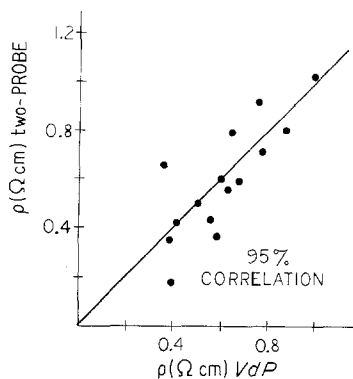
Figure 6 Values of resistivity obtained by the two-probe compared to the van der Pauw technique show a strong correlation (95%). Both techniques produce equivalent results.

Data suggest two optimum Magnex geometries. Large area samples should be moulded via a centre sprue with large sprue diameter. Also, long, thin samples are more uniform and provide a better shield to EMI. These can be laminated together to produce a larger sample. The effect of the lamination process is not discussed here, but it is a topic we are presently investigating.

We have also conducted a separate study to determine the reliability of the van der Pauw technique as a measuring tool. Resistivity data are taken using the van der Pauw technique and the more common two-probe technique. For this, we needed samples with uniform fibre density and orientation. We chose samples cut to include pieces 2 and 3 from the dog-bone. See Fig. 4. Point contacts were made at each corner, and van der Pauw data were collected. Two contacts were then inserted through each sample sideways, at a distance L apart. Voltage across the contacts for a constant current gives

$$(V/I) = 2R_c + \varrho L/A \qquad (8)$$

where A is the cross-sectional area and R_c is the contact resistance. After measuring the voltage, the contacts are relocated to a new distance L. Typical results of (V/I) against L are shown in Fig. 5. A linear regression is used to extract ϱ and R_c. Values of ϱ obtained by both methods are plotted in Fig. 6. A correlation of 95% shows that the two techniques produce equivalent results.

References

1. D. BIGG and D. STUTZ, *Polym. Compos.* **4** (1983) 40.
2. D. SOMMERS, *Polym. Plastic Technol. Engng* **23** (1984) 83.
3. L. J. VAN DER PAUW, *Philips Res. Rep.* **13** (1958) 1.
4. L. V. HMURCIK and M. R. KINSLER, *Bull. Amer. Phys. Soc.* **31** (1986) 1116.
5. S. AMER, *Solid State Electron.* **6** (1963) 141.
6. J. HORNSTRA and L. J. VAN DER PAUW, *J. Electron. Control* **1** (1959) 169.
7. J. C. NABLO, "Evaluation of Mitech Corporation Brunsmet Fiber Filled Placques", Brunswick Corporation, 2000 Brunswick Lane, Deland, Florida 32724 (1965).
8. W. L. PRICE, *Solid State Electron.* **16** (1973) 753.
9. J. DAVID and M. BUEHLER, *ibid* **20** (1977) 539.
10. W. VERSNEL, *ibid.* **21** (1978) 1261.
11. Bulletin 2-8406, Mitech Corporation, 4399 Hamaan Pky, Willoughby, Ohio 44094 (1983).
12. K. EVANS and A. GIBSON, *Compos. Sci. Technol.* **25** (1986) 149.
13. F. FOLGAR and C. TUCKER, *J. Reinf. Plast. Compos.* **3** (1984) 98.
14. J. HOBURG and J. DAVIS, *IEEE Trans. Educ.* **E-26** (1983) 138.
15. M. LOVRICH and C. TUCKER, Society of Plastics Engineers 43rd Annual Technical Conference (1985) (14 Fairfield Drive, Brookfield, Ctr. Connecticut 06850), p. 1119.
16. R. PRAKASH, *Compos.* **131** (July 1981).
17. W. ROSE, *Nature* **191** (1961) 242.
18. L. KLEINER, Society of Plastic Engineers Regional Technical Conference: EMI/RFI Shielding Plastics, Chicago, June 1982, (14 Fairfield Drive, Brookfield, Ctr. Connecticut 06850) p. 111.
19. J. GILLESPIE, J. VANDERSCHUREN and R. PIPES, *Polym. Compos.* **6** (1985) 82.
20. G. JEFFERY, *Proc. Roy. Soc.* **A102** (1922) 161.
21. D. BRIGHT, R. CROWSON and M. FOLKES, *J. Mater. Sci.* **13** (1978) 2497.
22. R. SHERMAN, L. MIDDLLEMAN and S. JACOBS, *Polym. Engng Sci.* **23** (1983) 36.
23. K. CHUNG, A. SABO and A. PICA, *J. Appl. Phys.* **53** (1982) 6867.